Theor Appl Climatol (2013) 112:227–241
DOI 10.1007/s00704-012-0729-4

ORIGINAL PAPER

Identification of the principal patterns of summer moisture transport in South America and their representation by WCRP/CMIP3 global climate models

Carla Gulizia · Inés Camilloni · Moira Doyle

Received: 11 January 2012 / Accepted: 12 July 2012 / Published online: 1 August 2012

Abstract The goal of this study is to assess the ability of a set of global climate models (GCMs) to represent the main regional spatial patterns of austral summer moisture transport in South America in order to evaluate if one of the possible causes of GCMs misestimating summer precipitation in this region could be associated with an erroneous representation of these patterns. For this purpose, NCEP/NCAR reanalysis and 20 GCMs from the WCRP/CMIP3 multi-model dataset for the period 1960–1999 were considered. Extreme cases of moisture transport patterns were selected to assess their association with rainfall anomalies. Results obtained indicate that only some aspects of water vapor transport and convergence in South America as well as the associated precipitation anomalies can be reproduced adequately by GCMs. Finally, a case study is presented showing that one of the moisture transport patterns identified was observed during December 2008–February 2009.

C. Gulizia · I. Camilloni · M. Doyle
Departamento de Ciencias de la Atmósfera y los Océanos,
Facultad de Ciencias Exactas y Naturales,
Universidad de Buenos Aires,
Buenos Aires, Argentina

C. Gulizia · I. Camilloni · M. Doyle
Centro de Investigaciones del Mar y la Atmósfera (CIMA),
Universidad de Buenos Aires-Consejo Nacional de
Investigaciones Científicas y Técnicas,
Buenos Aires, Argentina

C. Gulizia · I. Camilloni · M. Doyle
UMI IFAECI/CNRS,
Buenos Aires, Argentina

C. Gulizia (✉)
Departamento de Ciencias de la Atmósfera y los Océanos,
Facultad de Ciencias Exactas y Naturales,
Centro de Investigaciones del Mar y la Atmósfera (CIMA),
UMI IFAECI/CNRS, Universidad de Buenos Aires-CONICET,
Buenos Aires, Argentina
e-mail: gulizia@cima.fcen.uba.ar

1 Introduction

Climate change is considered one of the severest problems faced nowadays by humanity due to the magnitude of its economical, social, and ecological impacts. In particular, Southern South America has been identified as a region subject to climate trends that could be related to the increase of atmospheric concentration of greenhouse gases. Examples of changes are increased precipitation (Castañeda and Barros 1994; Giorgi 2002a; Berbery et al. 2006; Haylock et al. 2006; Re et al. 2006; Re and Barros 2009; Marengo et al. 2010) and river flows (Barros 2006; Camilloni 2007; Doyle and Barros 2011) as well as modifications of surface atmospheric circulation (Di Luca et al. 2006) and extreme temperatures (Rusticucci and Barrucand 2004; Marengo et al. 2010). Therefore, considering the variety of impacts of the observed trends, it is necessary to design adaptation measures in order to reduce the vulnerability of human and natural systems and to respond both to actual and possible future changes. However, for an effective adaption, the reduction of uncertainties of future scenarios is essential. Climate projections are elaborated using the most advanced global climate models (GCMs) since they are the most reliable tool available at present for simulating the processes that will determine future global or regional climate change. Nevertheless, GCMs are still unable to represent appropriately all processes of the climate system leading to projections with considerable

uncertainties. Therefore, validation studies are a relevant tool to estimate the reliability of future climate projections.

Precipitation occurrence depends essentially on the availability of atmospheric water vapor. The Amazon region, in which the main source of moisture is the tropical Atlantic Ocean, plays a fundamental role in its exchange between the tropics and extra-tropics and for the summer precipitation in South America (Marengo 1992; Herdies et al. 2002). The transport of tropical air to higher latitudes is closely linked to the Chaco low, through its impact on the South American low level jet (SALLJ, Herdies et al. 2002) and to the circulation associated with the semipermanent anticyclone over the South Atlantic Ocean. Two atmospheric circulation patterns which condition the distribution of South American summer precipitation have been identified by several authors, using different time periods and data (Nogués-Paegle and Mo 1997; Doyle and Barros 2002; Herdies et al. 2002; Grimm and Zilli 2009). The first pattern is characterized by a low-level continental tropical current with a zonal trajectory from the base of the Bolivian Andes to the Atlantic Ocean, carrying moisture to the South Atlantic Convergence Zone (SACZ). During this active phase of the SACZ, precipitation increases in this area, and a net moisture divergence is registered over southeastern South America (SESA) dominated by an anticyclonic circulation. As the flow exits the continent and enters the Atlantic Ocean, it merges with the anticyclone. Further south, it reenters the continent transporting water vapor inland as far as the mountain ranges region of western Argentina. The second pattern occurs when the SACZ is in its inactive phase. Moisture is advected by an intense meridional component from northwestern South America to SESA, associated with the SALLJ. On these occasions, the SACZ receives less water vapor, while net convergence leading to increased precipitation is registered in SESA. Moreover, Doyle et al. (2011) show that this intense northern low-level water vapor flow with two convergence cores, one over eastern Argentina, southern Brazil, and Uruguay, and the other over western Argentina, along with a weakened SACZ is associated with the more extreme precipitation months favoring the occurrence of mesoscale convective systems. In most of SESA, precipitation is due to these systems (Zipser et al. 2006), which act in daily scales and account for a great part of the total monthly precipitation.

Recently, several studies have evaluated the precipitation simulated by GCMs over the South American continent (Boulanger et al. 2007; Vera et al. 2009; Pesquero et al. 2010) or over subcontinental regions (Camilloni and Bidegain 2005; Silvestri and Vera 2008; Seth et al. 2009). They found that models tend to underestimate precipitation over central eastern Argentina and to overestimate it over the SACZ region. Seth et al. (2009) analyzed nine World Climate Research Programme/Coupled Model Intercomparison Project phase 3 (WCRP/CMIP3) GCMs to evaluate the future changes of the annual cycle of precipitation over continental South America south of 10°S and east of 60°W. Their analysis included, among other variables, the evaluation of the divergence of water vapor flow, showing that most models tend to overestimate moisture convergence during the austral summer months in the monsoon region (50°–60°W, 10°–20°S). They also found that there is a high discrepancy among models in SESA region, although convergence is captured by the ensemble. The limitations of the GCMs in simulating some climatic features on regional scale could have multiple causes, such as low spatial resolution and parameterizations of subgrid processes (Giorgi 2002b). The goal of this study is to assess the ability of a set of GCMs to represent the main regional spatial patterns of austral summer moisture transport in South America in order to evaluate if one of the possible causes of the deficiencies in estimating summer precipitation in southern South America could be associated with their erroneous representation. This is done by comparing the austral summer vertically integrated moisture transport patterns derived from the National Centers for Environmental Prediction/National Center for Atmospheric Research (NCEP/NCAR) reanalysis (Kalnay et al. 1996) and those from a set of 20 GCMs for the period 1960–1999. The comparison is made for one GCM individually and for the ensemble since different authors (Phillips and Gleckler 2006; Glecker et al. 2008; Vidal and Wade 2007, 2008; Pierce et al. 2009, Knutti et al. 2010; Weigel et al. 2010) suggest the multimodel ensemble as the most useful tool to reduce uncertainties associated with GCMs. As the present analysis explores the relation between moisture transport and precipitation based on monthly fields of all variables, some processes of smaller time scales could not be completely represented. Nevertheless, as it will be discussed in Section 3, the main features of the association between both variables are still evident when considering mean fields derived from daily or monthly data.

The paper is organized as follows: Section 2 describes the WCRP/CMIP3 dataset and observations considered. Section 3 presents the principal modes of vertically integrated moisture transport derived from NCEP/NCAR reanalysis and their relation with precipitation anomalies, and Section 4 evaluates the representation of the moisture transport and convergence as well as the associated rainfall by GCMs. Section 5 presents a case study, and Section 6 summarizes the main conclusions.

2 Data

Vertically integrated moisture transport between surface and 700 hPa for 1960–1999 is calculated considering sea level pressure, specific humidity (q), and horizontal winds (u,v) on standard pressure levels from the monthly NCEP/NCAR

reanalysis for the austral summer months (December, January, and February). Even though the focus of the present work is South America, moisture transport is calculated for a larger domain (20°W–100°W, 12.5°N–57.5°S) in order to include the adjacent oceanic regions. For the precipitation analysis over the continental area between 30°W–85°W and 0°–60°S, two different monthly gridded datasets were considered: NCEP/NCAR reanalysis (2.5°lat×2.5°lon) and the University of Delaware dataset (UDel) (Willmott and Matsura 2001) derived from rain gauge observations and with 0.5°lat×0.5°lon resolution.

Model simulations from 20 GCMs (Table 1) of the WCRP/CMIP3 multi-model dataset are analyzed. The evaluated variables are monthly precipitation and vertically integrated moisture transport and convergence, computed between surface and 700 hPa considering the same variables and months as in the reanalysis case. The GCMs horizontal resolutions vary between 1.1°–4° in latitude and 1.1°–5° in longitude and range between 18 and 56 atmospheric vertical levels. In order to facilitate the comparison between observations, NCEP/NCAR reanalysis, and GCM simulations, all variables were interpolated to a common 2.5°lat×2.5°lon grid using the Krigging method.

Due to the low resolution of both reanalysis and GCMs, some features of the regional circulation, such as the SALLJ, cannot be detected with precision. Therefore, the analysis in this work only makes reference to the northwestern low-level flow as an indicator of the possible presence of the SALLJ. Also, since information on a monthly basis is used, daily variability is not captured, and thus, results could show some differences from two South American atmospheric circulation patterns previously identified by different authors (Doyle and Barros 2002; Herdies et al. 2002).

3 Principal modes of vertically integrated moisture transport derived from NCEP/NCAR reanalysis and their relation with precipitation

To identify the principal patterns of vertically integrated moisture transport, a T-mode principal component analysis (PCA) method is applied to austral summer (December, January, and February) monthly fields over the study region for the 1960–1999 period. By definition, the first components of the PCA reflect the most frequent patterns, while those of higher order could correspond to sporadic meteorological situations. Since this work searches for the most

Table 1 CMIP3 GCMs employed in this analysis

Model ID, vintage	Sponsor(s), country	Atmosphere resolution	Ocean resolution
CCSM3, 2005	National Center of Atmospheric Research, USA	1.4°×1.4° L26	0.3°×1° L40
CGCM3.1(T47), 2005	Canadian Centre for Climate Modelling and Analysis, Canada	~2.8°×2.8° L31	1.9°×1.9° L29
CGCM3.1(T63), 2005		~1.9°×1.9° L31	0.9°×1.4° L29
CNRM-CM3, 2004	Metéo-France/Centre National de Recherches Météorologiques, France	~1.9°×1.9° L45	0.5°–2°×2° L31
CSIRO-MK3.0, 2001	Commonwealth Scientific and Industrial Research Organization (CSIRO) Atmospheric Research, Australia	~1.9°×1.9° L18	0.8°×1.9° L31
ECHAM5/MPI-OM, 2005	Max Planck Institute for Meteorology, Germany	~1.9°×1.9° L31	1.5°×1.5° L40
GFDL-CM2.0, 2005	U.S. Department of Commerce/National Oceanic and Atmospheric Administration (NOAA)/Geophysical Fluid Dynamics Laboratory (GFDL), USA	2.0°×2.5° L24	0.3°–1.0°×1.0°
GFDL-CM2.1, 2005		2.0°×2.5° L24	0.3°–1.0°×1.0°
GISS-AOM, 2004	National Aeronautics and Space Administration (NASA)/Goddard Institute for Space Studies (GISS), USA	3°×4° L12	3°×4° L16
GISS-EH, 2004		4°×5° L20	2°×2° L16
GISS-ER, 2004	NASA/GISS, USA	4°×5° L20	4°×5° L13
INGV-SXG	Instituto Nazionale di Geofisica e Vulcanologia, Italy	~1.1°×1.1° L19	1°–2°×2°
INM-CM3.0, 2004	Institute for Numerical Mathematics, Russia	4°×5° L21	2°×2.5° L33
IPSL-CM4, 2005	Institut Pierre Simon Laplace, France	2.5°×3.75° L19	2°×2° L31
MIROC3.2(hires), 2004	Center for Climate System Research (University of Tokyo), National Institute for Enviromental Studies, and Frontier Research Center for Global Change (JAMSTEC), Japan	~1.1°×1.1° L56	0.2°×0.3° L47
MIROC3.2(medres), 2004		~2.8°×2.8° L20	0.5°–1.4°×1.4° L43
MRI-CGCM2.3.2, 2003	Meteorological Research Institute, Japan	~2.8°×2.8° L30	0.5°–2.0°×2.5° L23
PCM, 1998	National Center for Atmospheric Research, USA	~2.8°×2.8° L26	0.5°–0.7°×1.1° L40
UKMO-HadCM3, 1997	Hadley Centre for Climate Prediction and Research/Met Office, UK	2.5°×3.75° L19	1.25°×1.25° L20
UKMO-HadGEM1, 2004		~1.3°×1.9° L38	0.3°–1.0°×1.0° L40

Sponsoring institutions as well as the horizontal and vertical resolution of the atmosphere and ocean models are listed. Horizontal resolution is expressed as degrees latitude by longitude. Vertical resolution (L) is the number of vertical levels

frequently observed moisture transport conditions, and not for infrequent cases, inclusion of the latter ones would not add relevant information and are not discussed.

There are several methods to determine the number of significant components that should be considered when applying the PCA method. Among those the following are used:

- The Kaiser method: The principal components with eigenvalues greater than 1 are retained. This means that the relation between the new variable and some of the original variables is significantly different from zero (Kaiser 1960).
- Explained variance: The components that altogether explain more than 80 % of the total variance are retained (Wilks 2006).

When applying the PCA to the NCEP/NCAR reanalysis moisture transport fields, it was found that the three first components fulfilled both the Kaiser and the explained variance method criteria. Figure 1 shows the spatial patterns represented by the first three principal components (PC) that altogether explain 93.7 % of the total variance. The first one (–PC1, Fig. 1a) explains the largest part of the overall variance (91.2 %) as it describes the mean field of the moisture transport. This pattern shows the south Atlantic and Pacific anticyclones centered on 30°S and the westerlies located south of 40°S. Furthermore, the branch of the tropical low-level water vapor flux has a southeasterly direction that converges in the vicinity of the SACZ, at about 20°S, with the southwestward transport carried by the winds of the South Atlantic high. PC2 (Fig. 1b) explains 1.6 % of the variance and is characterized by a flow from northwestern (NW) South America that turns zonal over central Brazil between 10°S and 15°S. Two opposed circulations over the Atlantic Ocean are also identified at approximately (40°S, 30°W) and (15°S, 30°W) that—accompanied by the flow from NW South America—generate important convergence over southeastern (SE) Brazil. On the other hand, moisture transport over Argentina is mainly from the south as water vapor comes from the Atlantic Ocean and enters the South American continent in central eastern Argentina favored by the cyclonic circulation over the Southern Atlantic Ocean. This flow moves northward across the continent with a SE–NW direction until it reaches Bolivia, where it converges with a tropical continental flow and returns to the ocean after passing almost zonally over central–western and SE Brazil.

The third component (–PC3, Fig. 1c), which explains 0.9 % of the variance, presents a closed anticyclonic circulation at around 20°S that incorporates moisture from the Atlantic Ocean along the coastline between 10°S and 25°S, and then penetrates the continent up to (15°S, 55°W) where it divides in two branches. One is directed to the south–southeast until it returns to the ocean, while the northern branch is opposed to the low-level tropical continental flow.

As discussed previously, the first principal component represents the mean field of vertically integrated moisture transport, while the higher order ones correspond to different disturbances of the mean circulation that highlight the main features of the spatial patterns of moisture transport. Consequently, to explore the relations between monthly precipitation anomalies and the principal modes of moisture transport, only PC2 and –PC3 are considered. For this purpose, extreme events are selected on the basis of their corresponding factor loadings (FL2 and FL3, respectively). The criteria used are:

- $FL2 \geq 0.15$
- $FL3 < -0.10$

These threshold values are set to include approximately 15 % of the total cases. For the selected events, the composites of the moisture transport and convergence fields as well as the associated precipitation anomalies are presented in Figs. 2 and 3, respectively. Rainfall anomalies related to the complete period are taken and tested using a mean difference test. Shaded areas in Fig. 3 indicate significant anomalies at the 90 % confidence level.

As this analysis is based on monthly fields of all variables, some processes of smaller scale could not be completely represented imposing a limitation on the unique correspondence between net convergence (divergence) and positive (negative) precipitation anomalies. Consequently, the consistency between the composites of the mean fields of vertically integrated moisture transport and convergence for the extreme cases of FL2 and FL3 derived from daily and monthly data is analyzed. The main feature that distinguishes them is that in some limited areas, the mean fields computed with monthly data exhibit a more intense convergence than the ones calculated with daily values (Figure not shown). Additionally, as it will be discussed below, in most cases, extreme precipitation anomalies can be reasonably explained by the transport and convergence of water vapor fields.

For the circulation pattern and associated moisture convergence corresponding to the composite of extreme events of FL2 (14 cases; Fig. 2a), a moisture input from the tropical Atlantic Ocean and its subsequent counterclockwise rotation showing a NW–SE direction towards central Brazil is identified. It then turns towards the Atlantic Ocean where it reaches the South Atlantic anticyclonic circulation producing stronger convergence than the one observed in the vicinity. In the corresponding NCEP/NCAR precipitation anomaly field (Fig. 3a), positive values are maxima at approximately 20°S (marked with full red circle in Fig. 3a), somewhat further north of the SACZ mean position but which might be explained by net moisture convergence

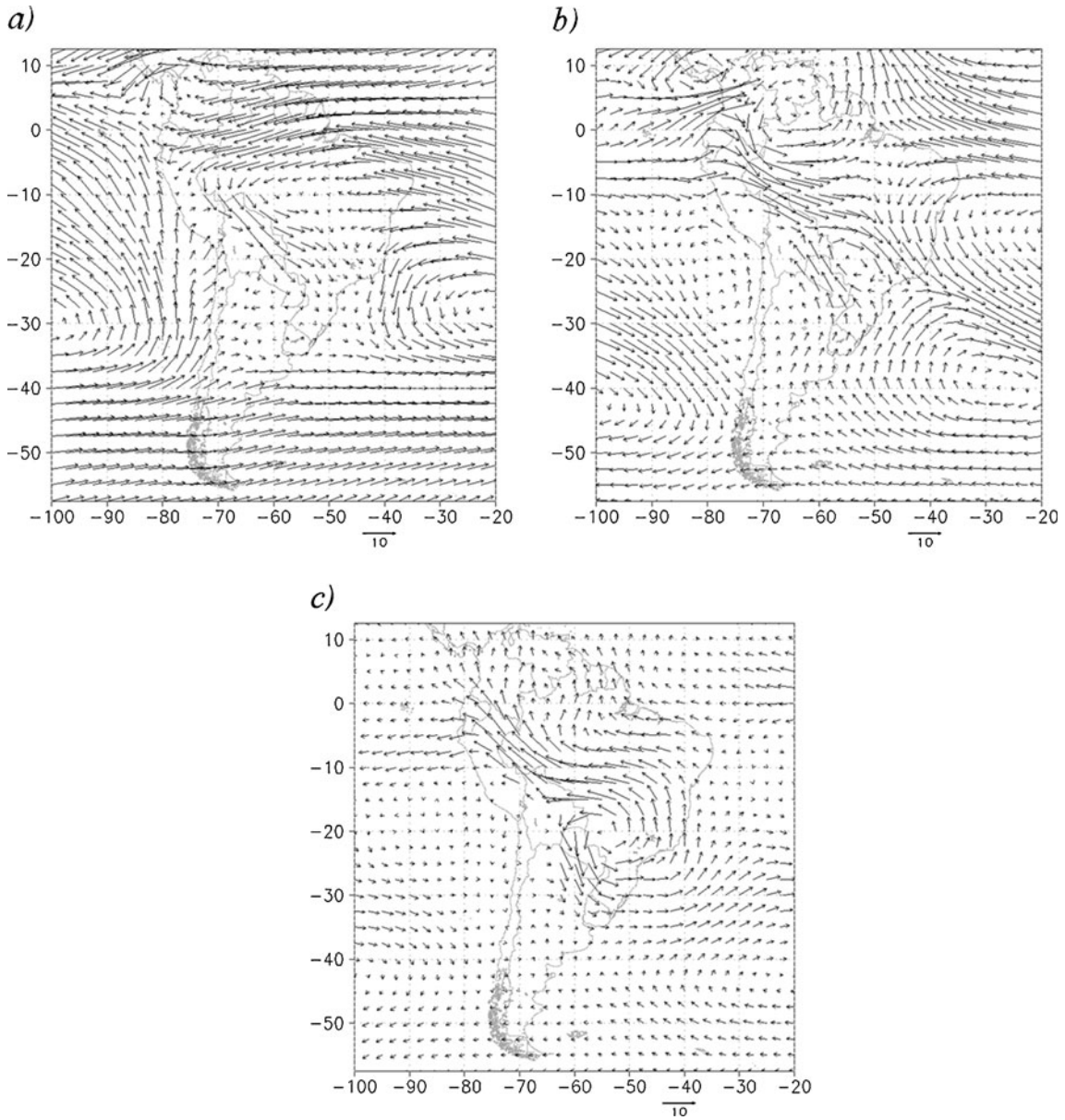

Fig. 1 First three principal components **a** –PC1, **b** PC2, **c** –PC3 of vertically integrated moisture transport for the austral summer months derived from the NCEP/NCAR reanalysis

in the SACZ area. Another region with positive precipitation anomalies is found south of 35°S. The zoom of Fig. 2a details the moisture entrance north of Uruguay through an anticyclonic circulation that reaches the Andes and finally joins the westerlies south of 35°S towards the Atlantic Ocean. In both cases, the positive precipitation anomalies are also captured by the UDel dataset (Fig. 3b). In the first region (full red circle in Fig. 3a), observations depict stronger anomalies than the reanalysis with the maximum values centered slightly northwards and hence extending over a larger statistically significant area. Over central and southern Argentina, the sign of observed rainfall anomalies is once again consistent with reanalysis though covering a larger area.

In most regions, there is physical consistency between NCEP/NCAR precipitation and water vapor transport and convergence data. However, it should be noted that in some cases, as in northern Brazil and on the east coast around 25° S, negative precipitation anomalies are not explained by the moisture transport since in these areas convergence is dominant (Fig. 2a). This could be in part due to the methodology employed in this study and some limitations that must be taken into account to analyze the results properly. For example, there is not necessarily a direct relationship between the occurrence of convergence and positive precipitation anomalies since rainfall can also be affected by evaporation, which is not studied here due to lack of observational data

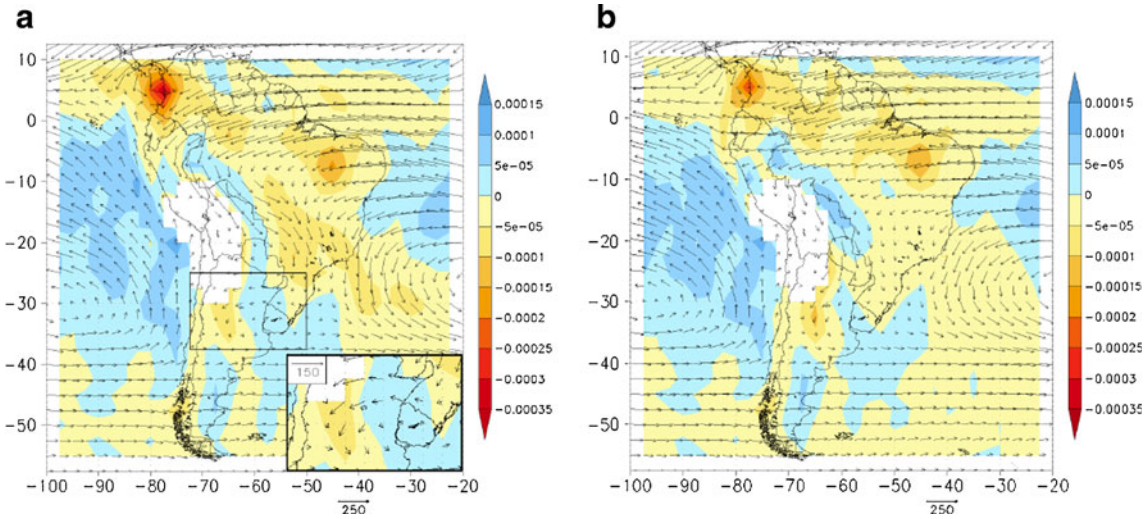

Fig. 2 Composites of the monthly extreme events of vertically integrated moisture transport (millimeters per meter per second) (vectors) and convergence (millimeters per second) (*shaded*) from the NCEP/NCAR reanalysis for **a** FL2 ≥0.15 and **b** FL3 < −0.10

on a continental scale. Also, due to the monthly time scale used, weak monthly convergence may not fully represent the daily events of the month. A number of days with divergence and others with convergence can occur during a month, and these could, on average, be compensated.

However, the comparison of the mean austral summer precipitation fields of both data sets sheds new light. Although anomalies follow similar patterns in both cases, there are some marked differences between the mean fields (Fig. 4). A minimum precipitation band appears east of the Andes in tropical latitudes in the reanalysis case which is consistent with divergence in the area and generated by modeled topography, but does not represent the observed precipitation field. During this season, the Amazon basin is characterized by maximum rainfall located in central Brazil (Fig. 4b); however, the highest values in the reanalysis rainfall field (Fig. 4a) are displaced northeastward. Hence, convergence values (Fig. 2a) are still high in this region because although precipitation anomalies are negative in this composite, the precipitation represented by reanalysis is still quite high compared to observations.

The composite of the moisture transport and convergence fields corresponding to extreme cases of FL3 (15 cases; Fig. 2b) shows that the continental zonal flow rotates at approximately 10°S and unlike in the previous case, crosses Bolivia and Paraguay with a more meridional orientation. The entrance of this flow over Argentina is accompanied by an anticyclonic rotation that runs along the Andes before leaving the continent between 35°S and 40°S. The moisture convergence, derived from the intersection of this flow and the South Atlantic anticyclone, occurs approximately in the same region as in the former case, approximately 25°S on the Brazilian eastern coast. It is also observed that the convergence regions on the Brazilian coast and in southwestern Argentina are in agreement with the maxima of NCEP/NCAR positive precipitation anomalies (full red circles in Fig. 3c), while the divergence over the eastern South American coast approximately between 30°S and 40° S (dashed red circle) concurs with negative precipitation anomalies. This same pattern is found in the composites of UDel precipitation (Fig. 3d); however, as in the previous case, there are some anomalies which cannot be explained by moisture transport and convergence fields. The relation between convergence and precipitation in northern South America as well as over the eastern coast south of 40°S is not straightforward. In the latter region, when analyzing the observed precipitation anomalies this could be attributed to the limited number of rainfall stations, thus making results difficult to assess. However, the NCEP/NCAR rainfall anomalies, independent of observed precipitation, present the same pattern. Therefore, monthly moisture transport and convergence do not seem to be the key mechanism responsible for the monthly rainfall anomalies in this case.

The area of positive anomalies in the UDel precipitation field (Fig. 3d) which encompasses the Atlantic coast in central Brazil, NE Argentina, central Paraguay, and the Atlantic coast of Argentina up to 40°S is not statistically significant given the high variability of rainfall in this region. However, despite the low statistical significance, the pattern is characteristic of SESA and is discussed in the case study presented in Section 5.

4 Representation of the vertically integrated moisture transport and associated precipitation by GCMs

This section presents a validation of the ability of the ensemble of 20 GCMs, and in particular of the model MRI-

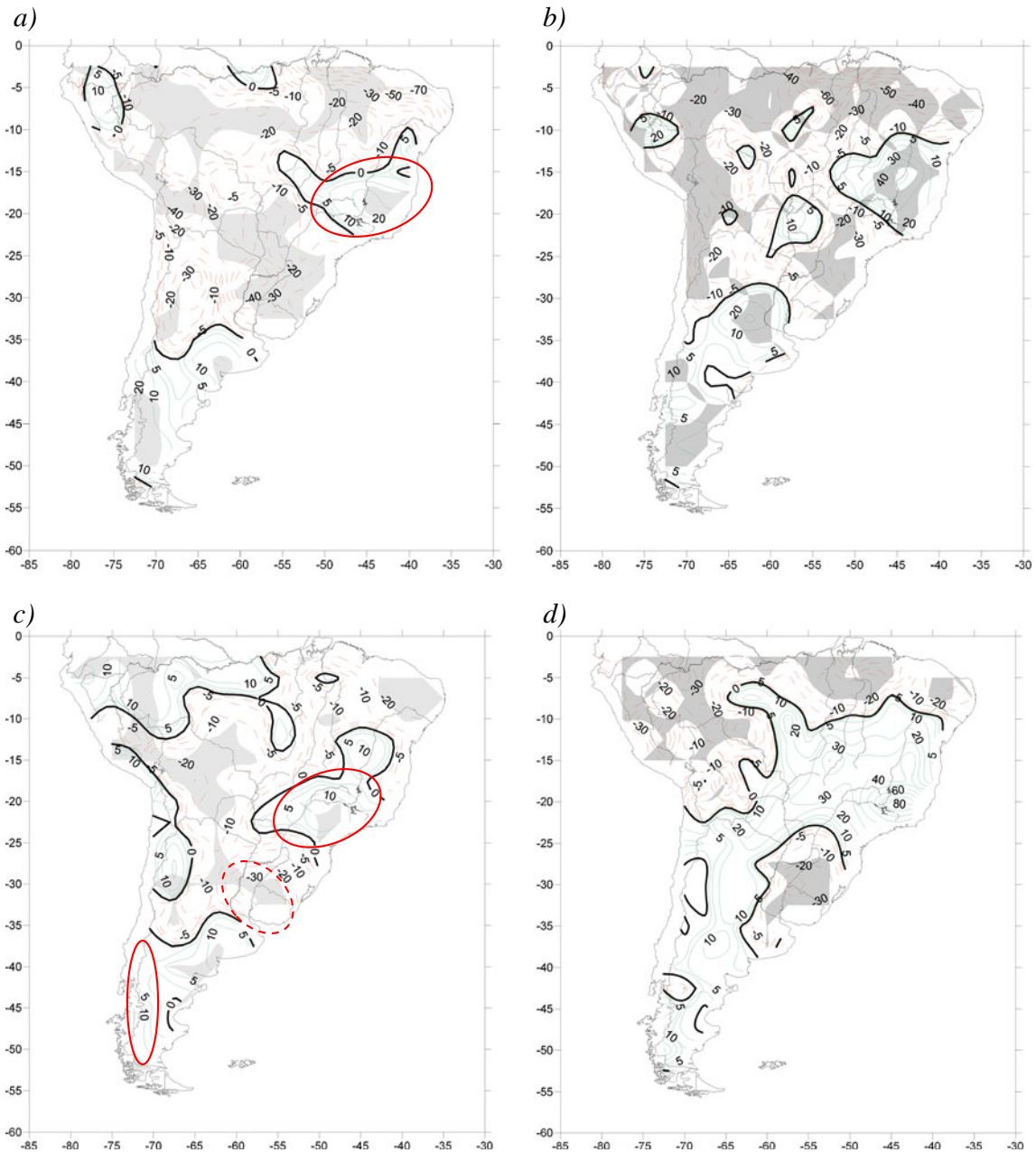

Fig. 3 Monthly precipitation anomalies (millimeters) derived from NCEP/NCAR reanalysis (**a**, **c**) and UDel dataset (**b**, **d**) for FL2 ≥0.15 (*upper panel*) and FL3 < −0.10 (*lower panel*). *Shaded areas* mark significant anomalies at the 90 % confidence level

CGCM2.3.2, to represent the structures found in the previous section. The selection of the MRI-CGCM2.3.2 model is based on a previous work by Gulizia et al. (2009), which shows that this model has an adequate representation of the summer precipitation field over South America on the basis of a statistically significant spatial correlation (R=0.76) between the observed and simulated fields. In this case, the explained variance by the first three principal components is 99.5 % (98.4, 1.0, and 0.1 %) for the ensemble and 95.4 % (93, 1.5, and 0.9 %) for MRI-CGCM2.3.2 model.

In the present case, the thresholds of the factor loadings considered for the selection of extreme cases differ from the ones selected for the reanalysis, and also between the different models. This is because both reanalysis and models have different correlation coefficients between their respective structures and the original variables.

Figure 5 shows the first three principal components for the ensemble of GCMs (EPCs). Pattern –EPC1 (Fig. 5a) adequately represents the mean moisture transport field during the austral summer months as well as the location of the southern Atlantic and Pacific anticyclones and the

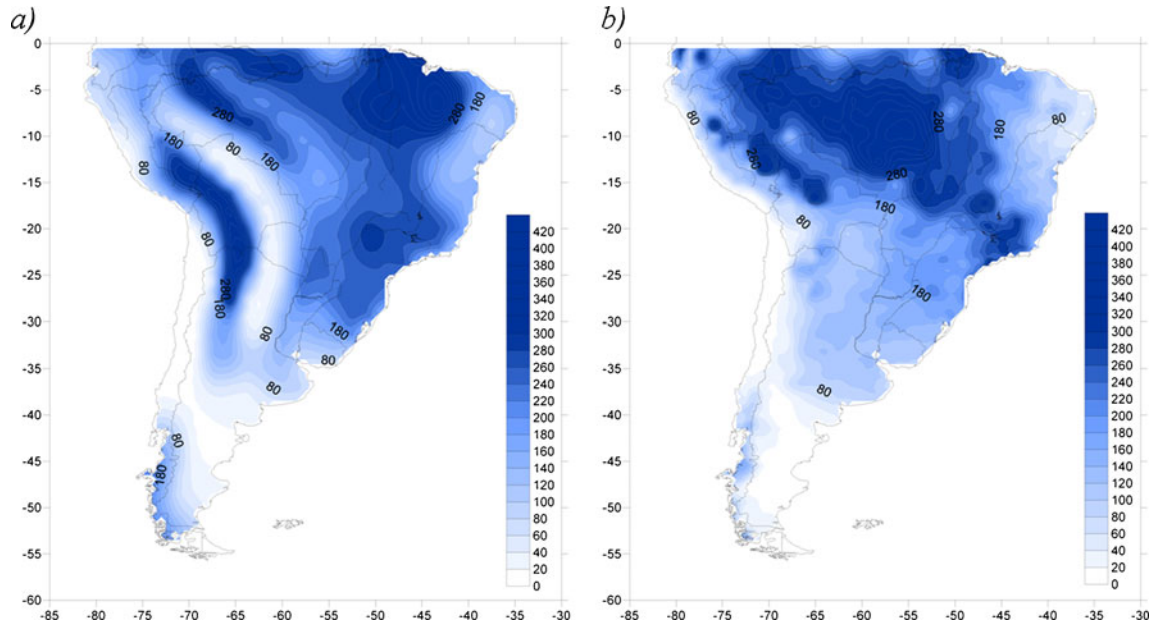

Fig. 4 Mean austral summer precipitation fields (millimeters): **a** NCEP/NCAR reanalysis and **b** UDel dataset

westerlies. Moreover, the incoming flow over Paraguay and Argentina has a similar position as in the mean flow derived from reanalysis (Fig. 1a).

Some of the aspects of the PC2 (Fig. 1b) are present in EPC2 (Fig. 5b). The gyres centered at 40°S over the Pacific and South Atlantic oceans in Fig. 1b are found in the spatial pattern of the ensemble although with less intensity. The flow confluence over the Atlantic Ocean observed in PC2 is slightly weaker in EPC2 while, on the contrary, the northwestern flow penetrating South America at 10°S and later passing through the north of Bolivia and Paraguay has a more intense meridional component. Likewise, EPC2 does not represent the incoming current in SE–NW direction over Paraguay and Bolivia present in PC2.

–PC3 (Fig. 1c) and –EPC3 (Fig. 5c) have some features in common. –EPC3 represents the zonal flux over Brazil that turns towards the NW of South America. However, the anticyclonic center located at 20°S observed in –PC3 is not clearly distinguishable in –EPC3.

Since EPC2 and to a lesser extent –EPC3 have certain features in common with PC2 and –PC3, respectively, the moisture transport and convergence as well as precipitation extreme cases composites obtained for reanalysis (Figs. 2 and 3) are compared with the ones of the ensemble of 20 GCMs (Figs. 6 and 7). However, given that the correlation coefficients between the original variables and the PCs differ in each of the analysis performed, new factor loading thresholds are used to select extreme cases, that is EFL2 $\geq$0.13 and EFL3 $<$ −0.013.

The composite of selected EPC2 events (Fig. 6a) shows that the semi-permanent subtropical anticyclones as well as the westerlies are adequately represented. However, the zonal component of the tropical current associated with the SALLJ is weaker in the ensemble. Moreover, the moisture flow branch running through the Brazilian territory has a less clear zonal component resulting not only in a slower flow over Paraguay but also over central–eastern Brazil and especially along the coast. The convergence over the coast of Brazil at 25°S in the ensemble is not as clear as in the reanalysis case appearing slightly displaced towards the interior of the continent.

In the composites of –EPC3 extreme events (Fig. 6b), the South Atlantic anticyclone enters the continent, while in the reanalysis case, it is located farther out over the ocean. The intersection of this anticyclonic circulation with the NW South American flow diverts the latter westward reducing its speed and leading to a weaker flow over north–central Argentina, thus creating a discrepancy between the ensemble and reanalysis patterns. Additionally, the flow over the eastern coast of Brazil is more intense for the ensemble of the 20 GCMs.

Figure 7 shows the composite of monthly precipitation anomaly fields from the ensemble of the 20 GCMs associated with extreme moisture transport and convergence presented in Fig. 6. The main feature of extreme events of EFL2 (Fig. 7a) is that rainfall anomalies in the SACZ region are much lower than in the pattern derived from NCEP/NCAR reanalysis (Fig. 3a), probably given the less intense zonal component in the low-level continental current. Likewise, positive precipitation anomalies appear over northern Argentina, Paraguay, and part of Bolivia covering a greater extension than in the reanalysis composite (Fig. 3a). This discrepancy in the coverage of the core of positive precipitation could be explained by a more

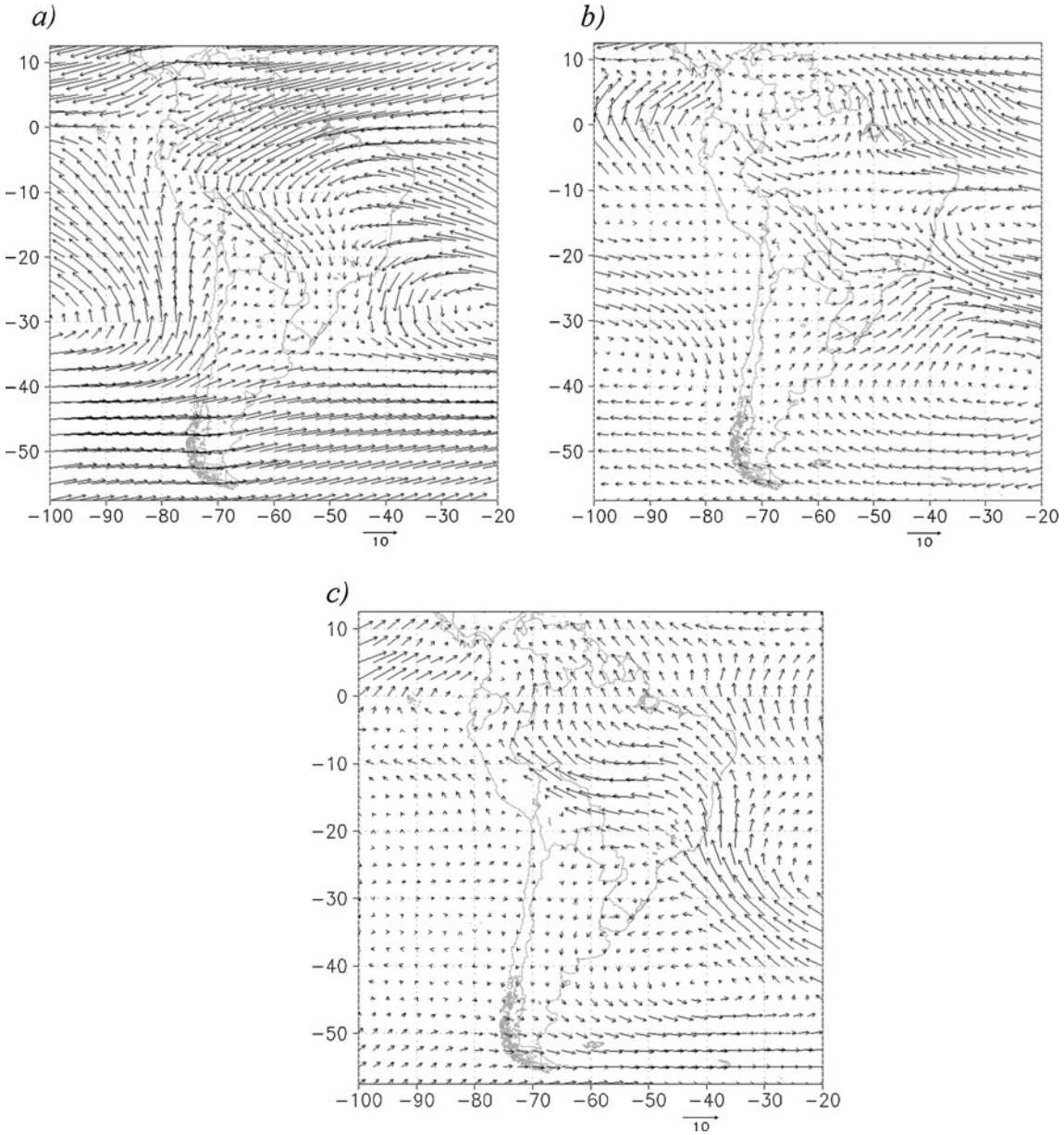

Fig. 5 First three principal components **a** –EPC1, **b** EPC2, and **c** –EPC3 of vertically integrated moisture transport for the austral summer months derived from the ensemble of 20 GCMs

meridional flux and stronger moisture convergence in the ensemble of GCMs than in the reanalysis field. In the case of –EPC3 extreme cases, the spatial distribution of precipitation anomalies is quite different from the composites derived from the observations probably due to the differences between the moisture transport fields described above.

Figure 8 shows the three main patterns resulting from a PCA on the MRI-CGCM2.3.2 monthly fields of vertically integrated moisture transport (–MPC1, MPC2, and –MPC3). Comparing Figs. 1a and 8a, it is clear that the –PC1 structure (Fig. 1a) is well represented by the –MPC1 one (Fig. 8a). Furthermore, MPC2 (Fig. 8b) reproduces the main features of PC2 (Fig. 1b), i.e., the two circulations in the Atlantic Ocean observed in PC2 are present in MPC2, although slightly shifted to the north. The low-level current flowing from NW South America towards the Atlantic Ocean is found in both structures; nonetheless, there is a difference in both patterns since in MPC2, the flow moves zonally out over the ocean, while in the reanalysis case, the entrance of the anticyclonic circulation over the continent shifts the zonal flow to a SE direction, hence exiting the continent farther south. The absence of the closed center in MPC2 contributes to a weaker flow over central–northern Argentina. Over the Pacific Ocean, the model exhibits a

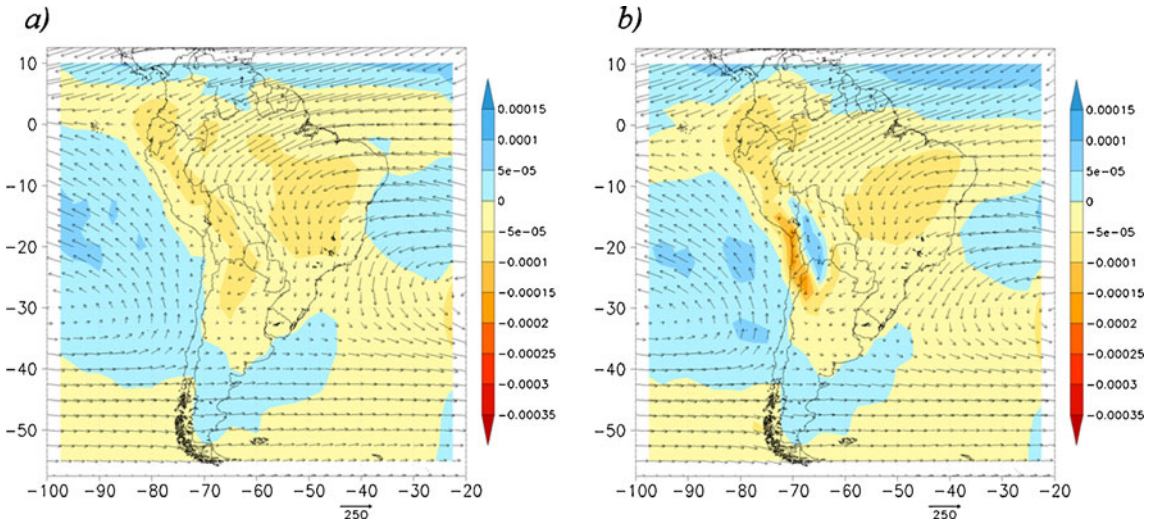

Fig. 6 Composites of the monthly extreme events of vertically integrated moisture transport (millimeters per meter per second) (vectors) and convergence (millimeters per second) (*shaded*) of vertically integrated moisture from the ensemble of 20 GCMs for **a** EFL2 ≥0.13 and **b** EFL3 < −0.013

cyclonic circulation shifted northward with respect to the reanalysis, and an anticyclonic system appears south of 40°S.

The MPC3 pattern (Fig. 8c) represents adequately the structure –PC3 (Fig. 1c) since the most outstanding feature, the counterclockwise gyre present over the continent in the reanalysis field, is located at approximately the same latitude, 20°S, though slightly shifted to the east. However, there is a difference over the Pacific Ocean given the intense closed circulation the model presents and which is noticeably weaker and displaced westward in the reanalysis pattern.

The thresholds established for selecting the extreme cases of the second and third principal components are MFL2 ≥0.15 and MFL3 ≥0.12. Figure 9 shows the moisture transport and convergence composites of MPC2 and MPC3 extreme events. In the first case (Fig. 9a), the anticyclonic circulations of the Pacific and Atlantic oceans are properly represented, even though the Pacific one is slightly weaker. This figure also indicates that the intensity and position of the moisture

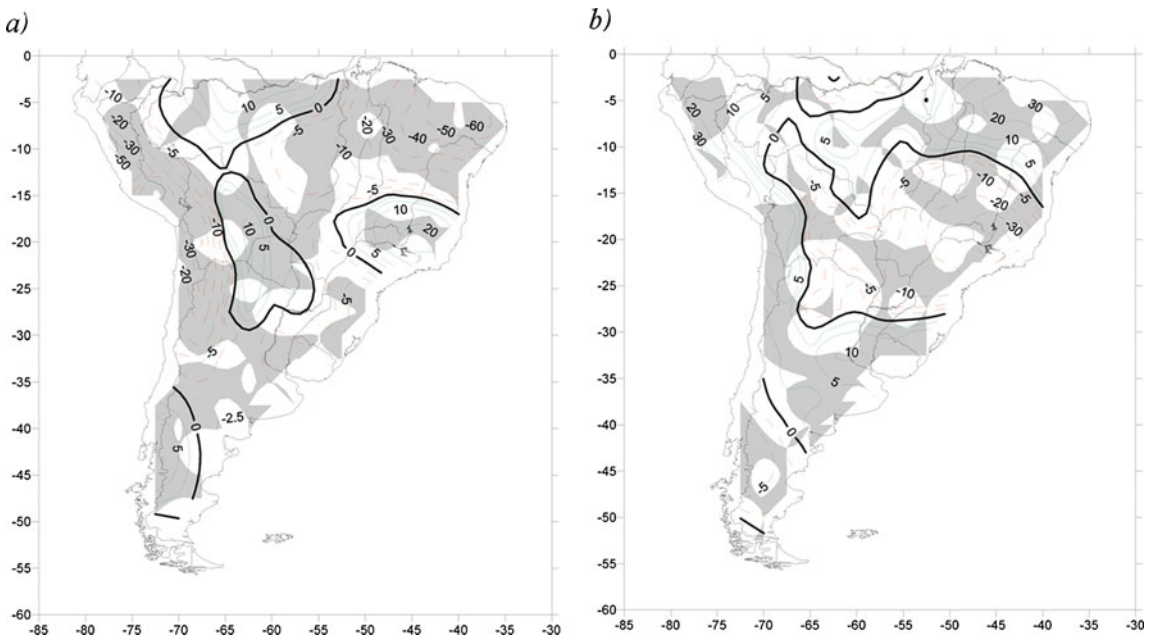

Fig. 7 Composites of the monthly precipitation anomalies (millimeters) of the GCMs ensemble for **a** EFL2 ≥0.13 y **b** EFL3 < −0.013. *Shaded areas* mark significant anomalies at the 90 % confidence level

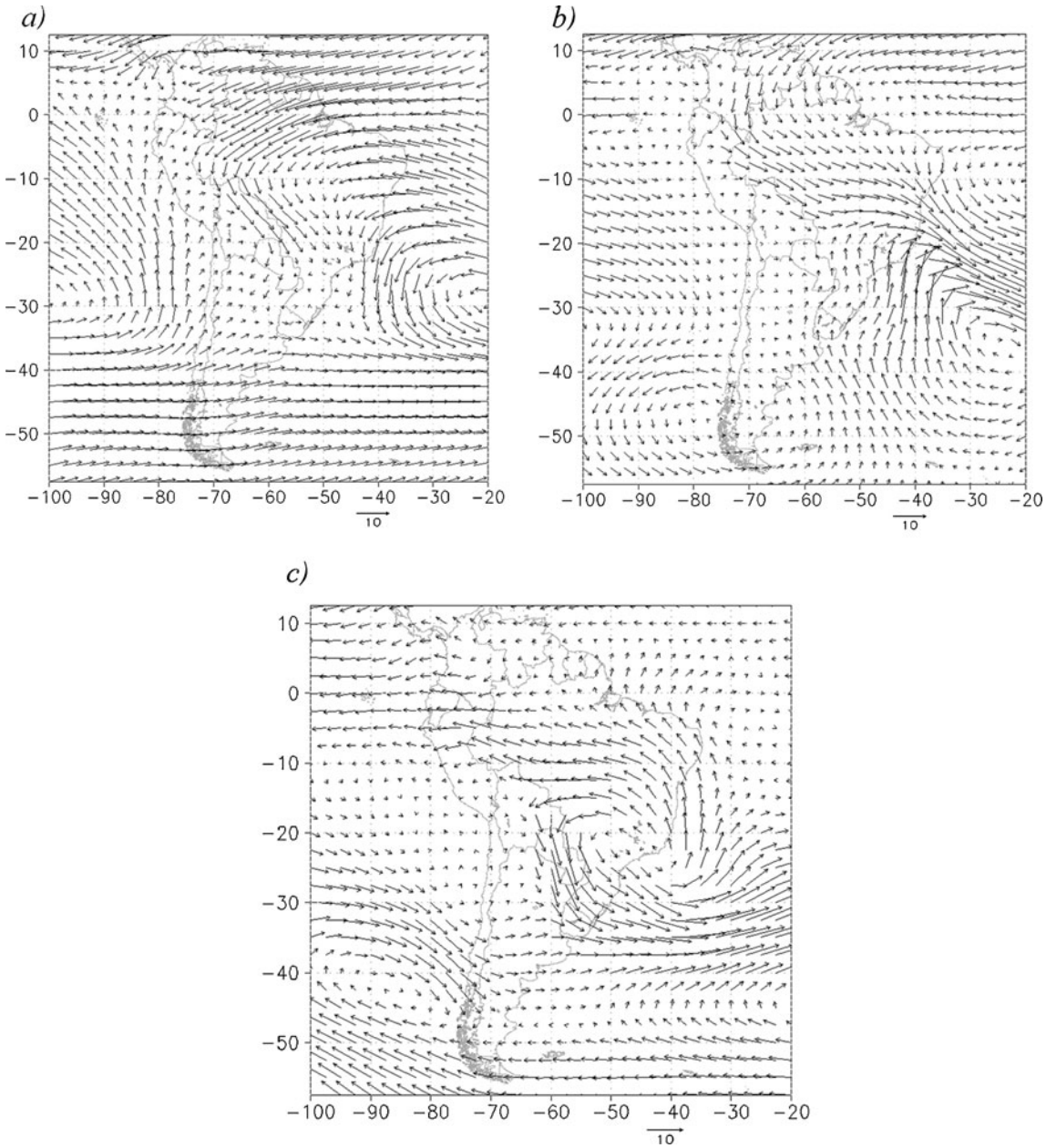

Fig. 8 Same as Fig. 5, but for MRI-CGCM2.3.2 **a** –MPC1, **b** MPC2, and **c** MPC3

transport carried out by the westerlies in the model are similar to the reanalysis, while the direction of the tropical current is less zonal (Fig. 2a). Nonetheless, the circulation over Argentina is well represented. Comparison between reanalysis and model composites for FL3 (Fig. 9b) reveals that the subtropical anticyclones, and the low level flux that crosses northern Bolivia towards Argentina, are adequately represented, while the flow along the SE coast of Brazil is slightly more intense in the model.

The composite of precipitation anomalies for MFL2 extreme events (Fig. 10a) is positive and of similar intensity over the SACZ region to those calculated from the UDel rainfall data (Fig. 3b). However, the precipitation distribution is very different from the observed pattern in the rest of the continent. Figure 10b shows that the sign of precipitation anomalies for MFL3 extreme cases is completely reversed between the model and observations (Fig. 3d), except south of 40°S where the anomalies of both composites are positive. These differences could be associated with the model moisture transport and convergence spatial pattern where the anticyclonic circulation enters the continent as far as 65°W accompanied by a significant southern transport that resembles the inactive SACZ phase with positive precipitation anomalies south of 25°S and negative to the north. The

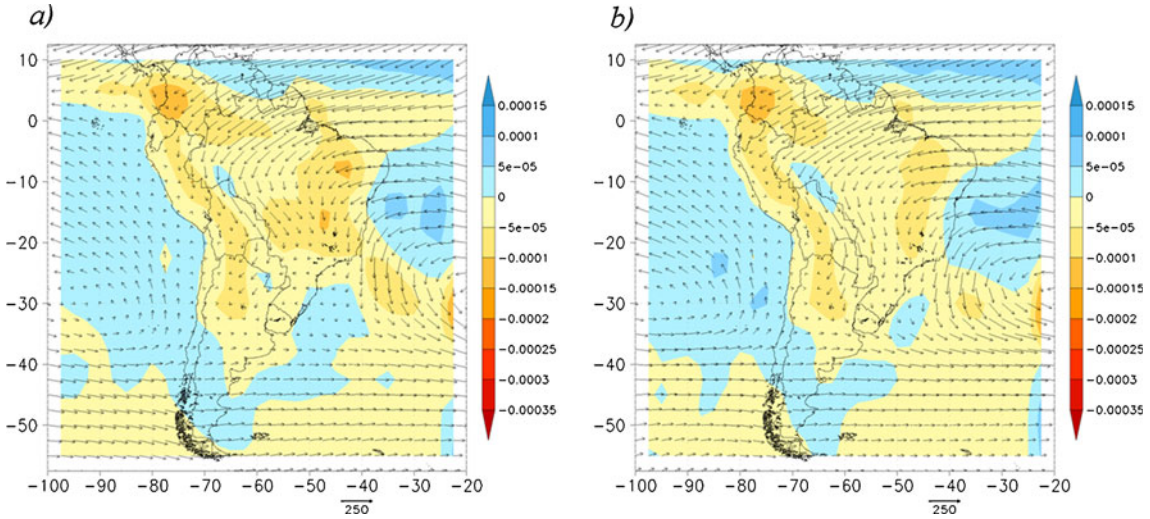

Fig. 9 Same as Fig. 6, but for MRI-CGCM2.3.2, **a** MFL2 ≥0.15 and **b** MFL3 ≥0.12

moisture transport field derived from the reanalysis does not show this anticyclonic circulation, while the meridional transport presents a curvature to the west like in the active SACZ phase.

5 Case study: December 2008–February 2009

Between November 2008 and February 2009, the monthly precipitation anomalies in southern South America were characterized by large dry regions in central–eastern Argentina which extended and deepened particularly throughout the Paraná basin during December 2008 (Fig. 11). On the other hand, in central–western Argentina, rainfall anomalies were positive during November and December 2008 and, at the same time, the SACZ region over the Brazilian coast north of 25°S was wetter than average (Fig. 11). The spatial distribution of rainfall anomalies that occurred during this period is of particular interest since it was accompanied by major social and economic impacts, primarily associated with water shortages with extended drought conditions that had begun months earlier in vast regions of Argentina.

The composites of precipitation anomalies for –PC3 extreme events (Fig. 3d) discussed in Section 3 show a spatial pattern similar to that observed between December 2008

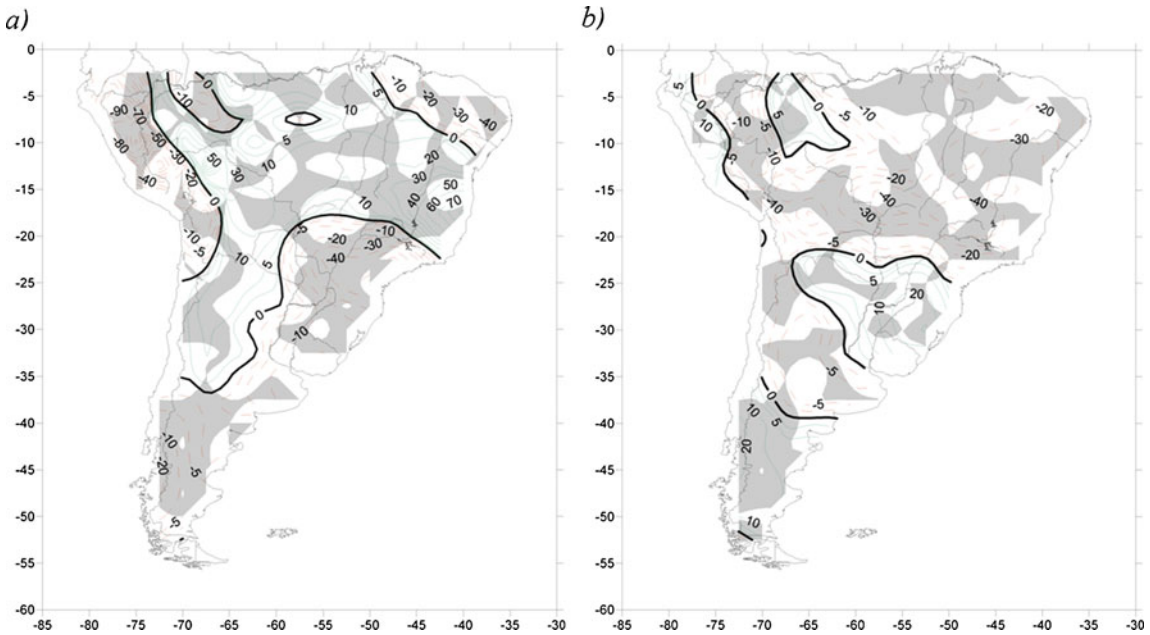

Fig. 10 Same as Fig. 7, but for MRI-CGCM2.3.2, **a** MFL2 ≥0.15 and **b** MFL3 ≥0.12

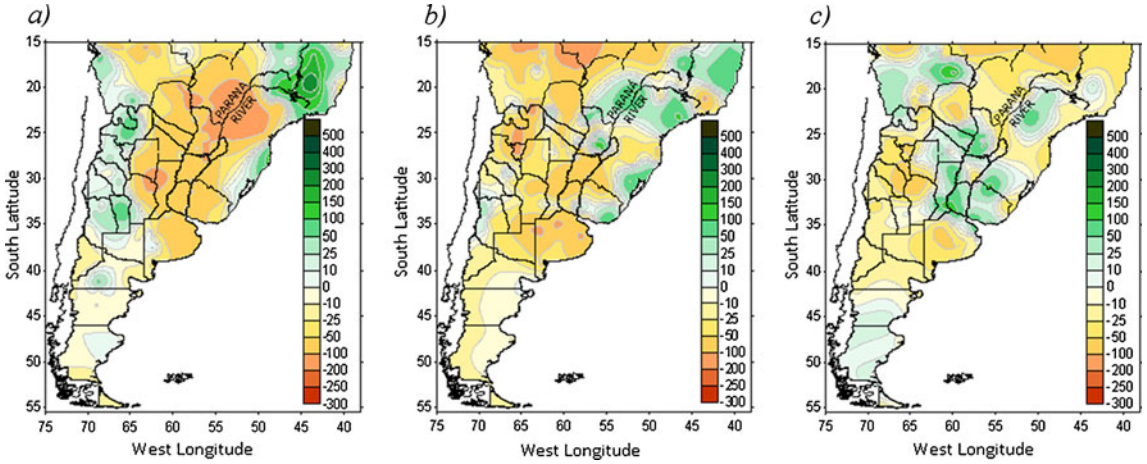

Fig. 11 Monthly mean precipitation anomalies (with respect to 1961–1990) for **a** December 2008, **b** January 2009, and **c** February 2009 (Source: National Weather Service, www.smn.gov.ar)

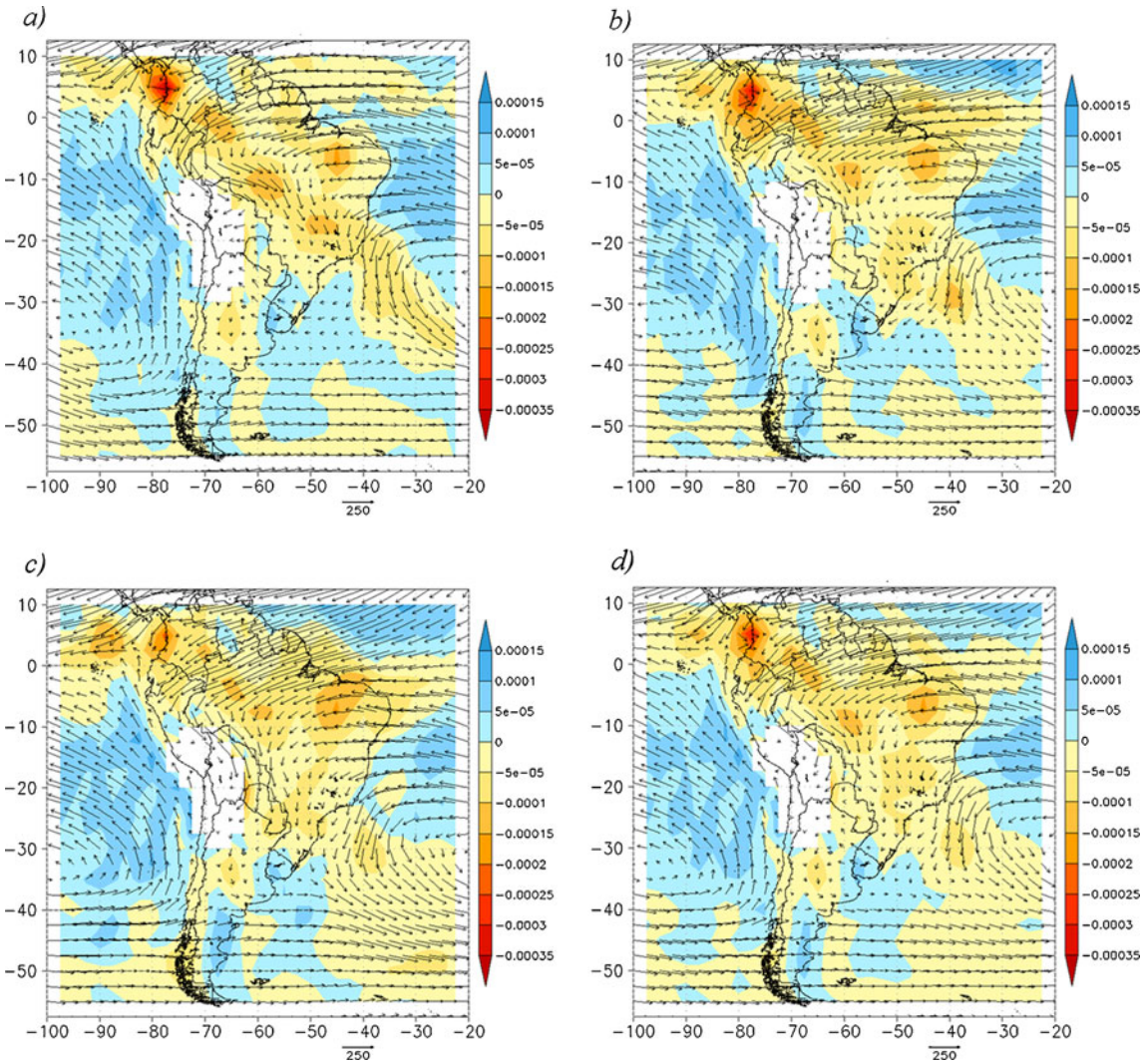

Fig. 12 Monthly mean fields of vertically integrated moisture transport (millimeters per meter per second) (vectors) and convergence (millimeters per second) (*shaded*) from the NCEP/NCAR reanalysis for **a** December 2008, **b** January 2009, **c** February 2009, and **d** the seasonal mean for the period December 2008–February 2009

and February 2009. Therefore, it is of interest to assess whether the moisture transport conditions that occurred during this period have some resemblance with the circulation features associated with this component.

Figure 12 shows the NCEP/NCAR reanalysis vertically integrated moisture transport and convergence monthly mean fields for the period December 2008–February 2009, for each individual month and for the three months average. It is found that the main features of the circulation in this period are similar to the spatial pattern –PC3 identified by the PCA method, both on the monthly and the seasonal scale. The two key features are:

- Moisture flows anticyclonically from the Atlantic Ocean through the eastern coast of South America at around 30°S, reaches the Andes, and completes the gyre exiting the continent south of 37.5°S. This flow could be associated with heavy rainfall in the west and scarce rains in eastern Argentina.
- Moisture flows through the South American continent from the NE towards the east of Brazil feeding the SACZ area and causing positive precipitation anomalies in that region.

6 Summary and conclusions

In this work, three austral summer patterns of vertically integrated moisture transport over South America derived from NCEP/NCAR reanalysis were identified using the PCA method for the period 1960–1999. The first principal component represents the mean field, whereas the second and third ones highlight some of the main features of the spatial patterns of moisture transport. This study focused on the analysis of these two latter components and the assessment of the ability of one GCM as well as an ensemble of 20 GCMs from the WRCP/CMIP3 database to represent them. Also, the rainfall anomaly fields derived from rain gauge data associated with the extreme cases of these modes were discussed in order to evaluate if one of the possible causes of GCMs misestimating summer precipitation in this region could be associated with an erroneous representation of these modes.

One of the patterns identified in the reanalysis data (PC2) is similar to the so-called intense or active SACZ (Nogués-Paegle and Mo 1997; Doyle and Barros 2002; Herdies et al. 2002; Grimm and Zilli 2009) that it is characterized by a tropical continental flow that deviates towards the SACZ and by a weakening of the Chaco Low (Fig. 1b). In the composite of extreme cases of this mode (Fig. 2a), the moist air coming from the Atlantic Ocean is accompanied by mostly negative rainfall anomalies in northeastern Argentina, southern Brazil, and Uruguay as over these regions the downward compensatory motion induced by the strong rise in the SACZ region prevails. However, when reaching the western mountains and foothills, these winds are forced to ascend and produce rainfall in central Argentina (Fig. 3b).

The other pattern (–PC3) shows the input of moisture into the continent from the Atlantic Ocean along the coastline between 10°S and 25°S through an anticyclonic circulation that divides into two branches at (15°S, 55°W), one of them with a south–southeastern direction and the other one opposed to the low-level tropical continental flow (Fig. 1c). The composite of extreme cases of this pattern (Fig. 2b) shows that these circulations are linked to heavy rainfall in the SACZ region and to a lesser extent in western Argentina and to dry conditions in southern Brazil, northern Uruguay, and eastern Argentina (Fig. 3d). Also, a similar pattern was registered during December 2008–February 2009, which deepened the drought conditions of previous months in large areas of central–eastern Argentina.

Only some of the aspects of vertically integrated austral summer moisture transport as well as the associated precipitation and water vapor convergence over South America are adequately reproduced by the ensemble of 20 GCMs and by the model MRI-CGCM2.3.2 individually. As moisture transport from tropics to extratropics is a key climate feature in South America and strongly determines both the spatial pattern and the sign of rainfall anomalies, its relatively erroneous representation explains at least partially the deficiencies of GCMs to estimate regional precipitation accurately. The analysis undertaken in this study does not systematically diagnose the physical explanation of model errors, but it suggests a possible pathway to improve model rainfall representation in South America. Meanwhile, in line with different authors (i.e., Pierce et al. 2009; Knutti et al. 2010; Weigel et al. 2010), we found that the multi-model ensemble results are more robust in the representation of observed fields strengthening the assumption that this is the most appropriate methodology to reduce uncertainties and to increase confidence in future climate projections.

Acknowledgments This research was supported by the University of Buenos Aires UBACYT-20020100100803, Consejo Nacional de Investigaciones Científicas y Técnicas PIP2009-00444, and Agencia Nacional de Promoción Científica y Tecnológica PICT07-00400. We acknowledge the Program for Climate Model Diagnosis and Intercomparison (PCMDI) for collecting and archiving the WCRP/CMIP3 model data.

References

Barros VR (2006) Tendencias climáticas e hidrológicas en la cuenca del Plata. In: Barros V, Clarke R, Silva Dias P (eds) El cambio climático en la Cuenca del Plata. CIMA, Buenos Aires, pp 12–18

Berbery EH, Doyle M, Barros V (2006) Tendencias regionales en la precipitación. In: Barros V, Clarke R, Silva Dias P (eds) El cambio climático en la Cuenca del Plata. CIMA, Buenos Aires, pp 67–79

Boulanger J-P, Martinez F, Segura EC (2007) Projection of future climate change conditions using IPCC simulations, neural networks and Bayesian statistics. Part 2: precipitation mean state and seasonal cycle in South America. Clim Dyn 28:255–271. doi:10.1007/s00382-006-0182-0

Camilloni I (2007) Tendencias hidrológicas en la Argentina. In: Barros V, Perczyk D (eds) Vulnerabilidad al cambio climático en Argentina. Secretaría de Ambiente y Desarrollo Sustentable de la Nación

Camilloni I, Bidegain M (2005) Escenarios climáticos para el siglo XXI. In: Barros V, Menéndez A, Nagy G (eds) El Cambio Climático en el Río de la Plata. CIMA, Buenos Aires, pp 33–39

Castañeda ME, Barros V (1994) Las tendencias de la precipitación en el Cono Sur de América al este de los Andes. Meteorológica 19:23–32

Di Luca A, Camilloni I, Barros V (2006) Sea-level pressure patterns in South America and the adjacent oceans in the IPCC AR4 Models. Preprints of 8th International Conference on Southern Hemisphere Meteorology and Oceanography. Foz de Iguaçu, Brazil

Doyle M, Barros V (2002) Midsummer low-level circulation and precipitation in subtropical South America and related sea surface temperature anomalies in the South Atlantic. J Climate 15:3394–3410

Doyle M, Barros V (2011) Attribution of the river flow growth in the Plata Basin. Int J Climatol 31:2234–2248. doi:10.1002/joc.2228

Doyle M, Saurral R, Barros V (2011) Trends in the distributions of aggregated monthly precipitation over the Plata Basin. Int J Climatol. doi:10.1002/joc.2429

Giorgi F (2002a) Variability and trends of sub-continental scale surface climate in the twentieth century. Part I: observations. Clim Dyn 18:675–691

Giorgi F (2002b) Variability and trends of sub-continental scale surface climate in the twentieth century. Part II: AOGCM simulations. Clim Dyn 18:693–708

Gleckler PJ, Taylor KE, Doutriaux C (2008) Performance metrics for climate models. J Geophys Res 113:D06104. doi:10.1029/2007JD008972, Atmospheres

Grimm A, Zilli M (2009) Interannual variability and seasonal evolution of summer monsoon rainfall in South America. J Climate 22:2257–2275

Gulizia C, Camilloni I, Doyle M (2009) Representation of precipitation and moisture transport in southern South America in the WCRP CMIP3 Multi-Model Dataset. Preprints of 9th International Conference on Southern Hemisphere Meteorology and Oceanography, Melbourne, Australia. http://www.bom.gov.au/events/9icshmo/poster_4.shtml. Accessed 23 July 2012

Haylock MR, Peterson TC, Alves LM, Ambrizzi T, Anunciação YMT, Baez J, Barros VR, Berlato MA, Bidegain M, Coronel G, Corradi V, Garcia VJ, Grimm AM, Karoly D, Marengo JA, Marino MB, Moncunill DF, Nechet D, Quintana J, Rebello E, Rusticucci M, Santos JL, Trebejo I, Vincent LA (2006) Trends in total and extreme South American rainfall in 1960–2000 and links with sea surface temperature. J Climate 19:1490–1512

Herdies DL, Da Silva A, Silva Dias MAF, Nieto Ferreira R (2002) Moisture budget of the bimodal pattern of the summer circulation over South America. J Geophys Res (Atmospheres) 107 (D20):8075. doi:10.1029/2001JD000997

Kaiser HF (1960) The application of electronic computers to factor analysis. Educ Psychol Meas 20:141–151

Kalnay E, Kanamitsu M, Kistler R, Collins W, Deaven D, Gandin L, Iredell M, Saha S, White G, Woollen J, Zhu Y, Chelliah M, Ebisuzaki W, Higgins W, Janowiak J, Mo KC, Ropelewski C, Wang J, Leetmaa A, Reynolds R, Jenne R, Joseph D (1996) The NCEP/NCAR 40-year reanalysis project. Bull Am Meteorol Soc 77:437–471

Knutti R, Abramowitz G, Collins M, Eyring V, Gleckler PJ, Hewitson B, Mearns L (2010) Good practice guidance paper on assessing and combining multi model climate projections. In: Stocker TF, Qin D, Plattner G-K, Tignor M, Midgley PM (eds) Meeting report of the Intergovernmental Panel on Climate Change expert meeting on assessing and combining multi model climate projections. IPCC Working Group I Technical Support Unit, University of Bern, Bern

Marengo JA (1992) Interannual variability of surface climate in the Amazon basin. Int J Climatol 12:853–863

Marengo JA, Rusticucci M, Penalba O, Renom M (2010) An intercomparison of observed and simulated extreme rainfall and temperature events during the last half of the twentieth century: part 2: historical trends. Clim Chang 98:509–529

Nogués-Paegle J, Mo KC (1997) Alternating wet and dry conditions over South America during summer. Mon Weather Rev 125:279–291

Pesquero JF, Chou SC, Nobre CA, Marengo JÁ (2010) Climate downscaling over South America for 1961–1970 using the Eta Model. Theor Appl Climatol 99:75–93

Phillips TJ, Gleckler PJ (2006) Evaluation of continental precipitation in 20th century climate simulations: the utility of multimodel statistics. Water Resour Res 42:W03202. doi:10.1029/2005WR004313

Pierce DW, Barnett TP, Santer BD, Gleckler PJ (2009) Selecting global climate models for regional climate change studies. Proc Natl Acad Sci U S A 106(21):8441–8446. doi:10.1073/pnas.0900094106

Re M, Barros V (2009) Extreme rainfalls in SE South America. Clim Chang 96:119–136

Re M, Saurral R, Barros V (2006) Extreme precipitations in Argentina. Proceedings of the 8th International Conference on Southern Hemisphere Meteorology and Oceanography, AMS. Foz do Iguaçu, Brazil, pp 1575–1584

Rusticucci M, Barrucand M (2004) Observed trends and changes in temperature extremes over Argentina. J Climate 17:4099–4107

Seth A, Rojas M, Rauscher S (2009) CMIP3 projected changes in the annual cycle of the South American Monsoon. Clim Chang. doi:10.1007/s10584-009-9736-6

Silvestri G, Vera C (2008) Evaluation of the WCRP-CMIP3 model simulations in the La Plata basin. Meteorol Appl 15:497–502

Vera C, González P, Silvestri G (2009) About uncertainties WCRP/CMIP3 climate simulations over South America. Preprints of the 9th International Conference on Southern Hemisphere Meteorology and Oceanography, Melbourne, Australia

Vidal J-P, Wade S (2007) A framework for developing high-resolution multi-model climate projections: 21st century scenarios for the UK. Int J Climatol 28:843–858

Vidal J-P, Wade S (2008) Multimodel projections of catchment-scale precipitation regime. J Hydrol 353:143–158

Weigel AP, Knutti R, Liniger MA, Appenzeller C (2010) Risks of model weighting in multimodel climate projections. J Climate 23:4175–4191

Wilks D (2006) Statistical methods in the atmospheric sciences, 2nd edn. Academic, London, p 627

Willmott CJ, Matsura K (2001) Terrestrial air temperature and precipitation monthly and annual time series (1950–1999) version 1.02. http://climate.geog.udel.edu/~climate/html_pages/precip_ts2.html. Accessed 23 July 2012

Zipser E, Liu C, Cecil DJ, Nesbitt SW, Yorty DP (2006) Where are the most intense thunderstorms on Earth? Bull Am Meteorol Soc 87:1057–1071